Crystal structure of BaMnB$_2$O$_5$ containing structurally isolated manganese oxide sheets

**Elizabeth M. Maschmeyer,[a] Liurukara D. Sanjeewa[b] and Kulugammana G. S. Ranmohotti[a]***

[a]Division of Chemistry and Biological Sciences, Governors State University, 1 University Parkway, University Park, IL 60484-0975, USA, and [b]Department of Chemistry, Clemson University, Clemson, SC 29634-0973, USA. *Correspondence e-mail: kranmohotti@govst.edu

In an attempt to search for mixed alkaline-earth and transition metal pyroborates, the title compound, barium manganese(II) pyroborate, has been synthesized by employing a flux method. The structure of BaMnB$_2$O$_5$ is composed of MnO$_5$ square pyramids that form Mn$_2$O$_8$ dimers by edge-sharing and of pyroborate units ([B$_2$O$_5$]$^{4-}$) that are composed of two corner-sharing trigonal–planar BO$_3$ units. These building blocks share corners to form $^2_\infty$[MnB$_2$O$_5$]$^{2-}$ layers extending parallel to (100). The Ba^{2+} cations reside in the gap between two manganese pyroborate slabs with a coordination number of nine. The title compound forms an interesting spiral framework propagating along the 2$_1$ screw axis. The structure is characterized by two alternating layers, which is relatively rare among known transition-metal-based pyroborate compounds.

1. Chemical context

Numerous borates with various crystal structures and compositions have been widely investigated over the last few decades (Heller *et al.*, 1986). Pyroborates containing the (B$_2$O$_5$)$^{4-}$ anion were first structurally characterized in 1950 (Berger, 1950). Pyroborates can be divided into two subclasses such as alkaline-earth-based pyroborates with general formula A_2B$_2$O$_5$ (A = alkaline earth metal) and transition-metal-based pyroborates with general formula MM'B$_2$O$_5$. If $M = M'$, the pyroborate is considered to be homo-metallic, otherwise it is hetero-metallic.

Alkaline-earth-based pyroborates adopt different structure types. During the investigation of the BaO/B$_2$O$_3$ system, Hubner revealed Ba$_2$B$_2$O$_5$ crystallizing in space group $P2/m$ (Hubner, 1969). The other alkaline-earth-based A_2B$_2$O$_5$ pyroborates (A = Mg, Ca, Sr) have been synthesized by high-temperature solid-state reactions. Mg$_2$B$_2$O$_5$ (Guo *et al.*, 1995*b*) crystallizes in space group $P2_1/c$. Ca$_2$B$_2$O$_5$ (Lin *et al.*, 1999*a*) and Sr$_2$B$_2$O$_5$ (Lin *et al.*, 1999*b*) are isotypic and crystallize in the same space group type as Mg$_2$B$_2$O$_5$ but have a different structure from the latter. Additionally, there exists a triclinic magnesium pyroborate ($P\bar{1}$; Guo *et al.*, 1995*a*). The existence of mixed alkaline-earth-based pyroborates (AA'B$_2$O$_5$) has been proven by the study of naturally occurring minerals. The crystal structures of two polymorphs of CaMgB$_2$O$_5$, kurchatovite and clinokurchatovite, have been originally determined in space group types $Pc2_1b$ (Yakubovich *et al.*, 1976) and $P2_1/c$ (Simonov *et al.*, 1980). However, the crystal structures of both minerals have been re-examined and refined in different space

OPEN ACCESS

http://dx.doi.org/10.1107/S2056989016013074 **1315**
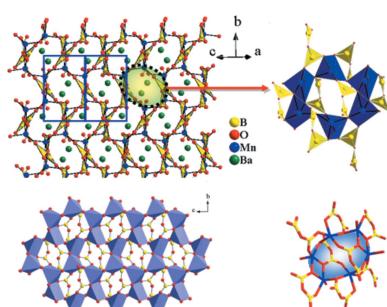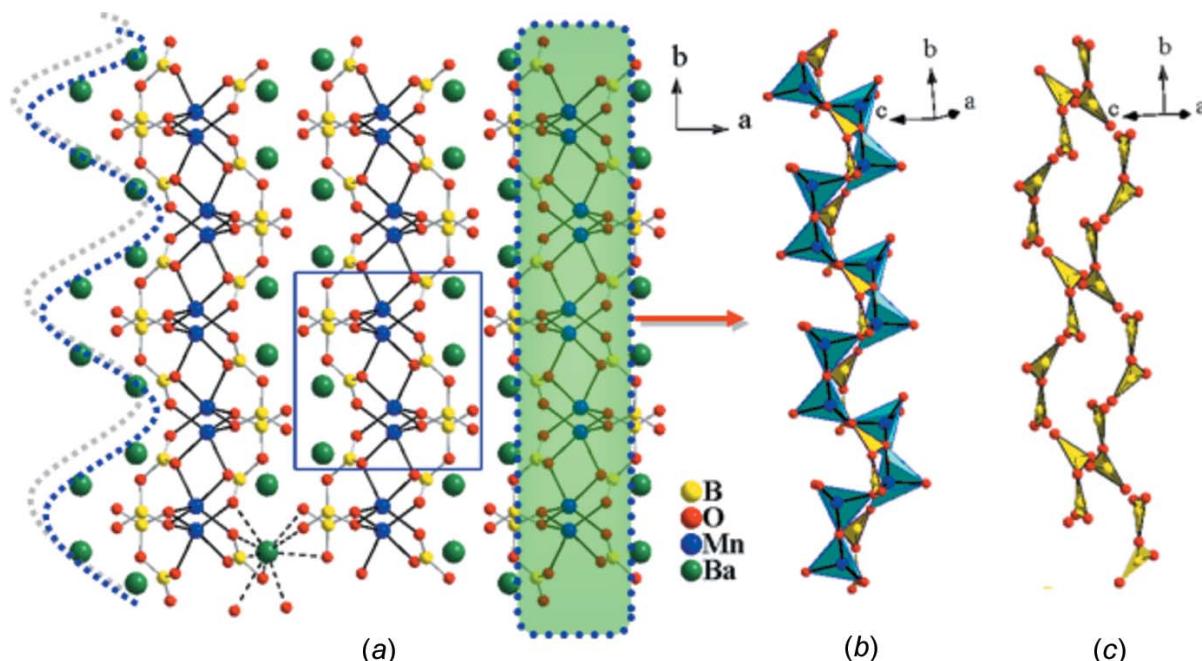
Figure 1
(*a*) Perspective view of the structure of BaMnB$_2$O$_5$ viewed along the *c* axis. The wavy and dotted line (left) indicates the zigzag arrays of Ba atoms. Only one Ba atom with bonds is drawn for clarity, demonstrating the function of Ba—O bonds with regard to holding neighboring [MnB$_2$O$_5$]$^{2-}$ slabs. (*b*) Polyhedral representation showing the $^2_\infty$[MnB$_2$O$_5$]$^{2-}$ spiral framework centered around the 2$_1$ screw axis of the unit cell. (*c*) Polyhedral representation showing the arrangement of isolated pyroborate units viewed approximately along the [101] direction.

group types (Callegari *et al.*, 2003). Based on these models, kurchatovite crystallizes in space group type *Pbca* whilst clinokurchatovite crystallizes in space group type *P*2$_1$/*c*.

Investigations of transition-metal-based homo-metallic pyroborates, M_2B$_2$O$_5$ have led to four compounds, namely Mn$_2$B$_2$O$_5$ (Sarrat *et al.*, 2005), Co$_2$B$_2$O$_5$ (Rowsell *et al.*, 2003), Cd$_2$B$_2$O$_5$ (Weil, 2003), and Fe$_2$B$_2$O$_5$ (Neumair & Huppertz, 2009). These phases crystallize isotypically with the triclinic form of Mg$_2$B$_2$O$_5$ (Guo *et al.*, 1995*a*). Efforts have been made to isolate transition-metal-based hetero-metallic phases, MM'B$_2$O$_5$. This has resulted in the synthesis of MnCoB$_2$O$_5$ and MnMgB$_2$O$_5$ (Utzolino & Bluhm, 1996), and Ni$_{1.5}$Zn$_{0.5}$B$_2$O$_5$ and Co$_{1.5}$Zn$_{0.5}$B$_2$O$_5$ (Busche & Bluhm, 1995). These structures are also isotypic with the triclinic form of Mg$_2$B$_2$O$_5$.

Investigations of the BaO/CuO/B$_2$O$_3$ phase diagram has resulted in the isolation of a non-centrosymmetric pyroborate, BaCuB$_2$O$_5$ (Smith & Keszler, 1997) with a unique structure type in space group type *C*2. As part of an effort to isolate new mixed alkaline earth and transition metal pyroborates, we have investigated the BaO/MnO/B$_2$O$_3$ phase diagram. In this study, we have grown single crystals of BaMnB$_2$O$_5$ and analyzed its crystal structure.

2. Structural commentary

The crystal structure of BaMnB$_2$O$_5$ defines a new structure type that can be described as being composed of manganese pyroborate slabs with composition $^2_\infty$[MnB$_2$O$_5$]$^{2-}$ that extend parallel to (100). Fig. 1*a* shows a perspective drawing of the BaMnB$_2$O$_5$ structure with the quasi-two-dimensional lattice

characterized by [MnB$_2$O$_5$]$^{2-}$ slabs. The barium cations reside between the parallel slabs and maintain the interslab connectivity through coordination to nine oxygen atoms (Fig. 2*c*).

Two non-equivalent boron atoms are present in the structure; both are surrounded by three oxygen atoms to form almost regular trigonal–planar units. As depicted in Fig. 2*b*, the isolated [B$_2$O$_5$]$^{4-}$ pyroborate groups are composed of two corner-sharing trigonal–planar BO$_3$ units. In the reported pyroborate structures (Thompson *et al.*, 1991), the terminal BO$_2$ planes pivot about the torsion angles to afford deviations from coplanarity that can range from 0 to 76.8° where the B—O—B angle ranges from 112 to 180°. In BaMnB$_2$O$_5$, the pyroborate groups show closely related geometric features as previously noted (Thompson *et al.*, 1991), exhibiting a B—O—B angle of 125.1 (5)° whilst the dihedral angle between the two BO$_3$ units within the pyroborate group is 48.62 (8)°. The
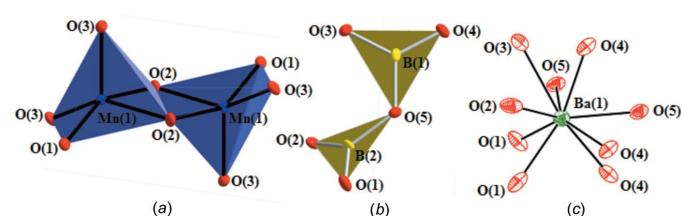
Figure 2
(*a*) Partial structure showing Mn$_2$O$_8$ dimers (polyhedral drawing). The apical oxygen, O3, in each MnO$_5$ square pyramid points in opposite directions. (*b*) Corner-sharing BO$_3$ groups forming a pyroborate unit. The BO$_3$ units within the pyroborate group are linked through a common O atom, O5. (*c*) The barium cation resides in a BaO$_9$ environment. Anisotropic displacement parameters are drawn at 95% probability.

(a)

(b)
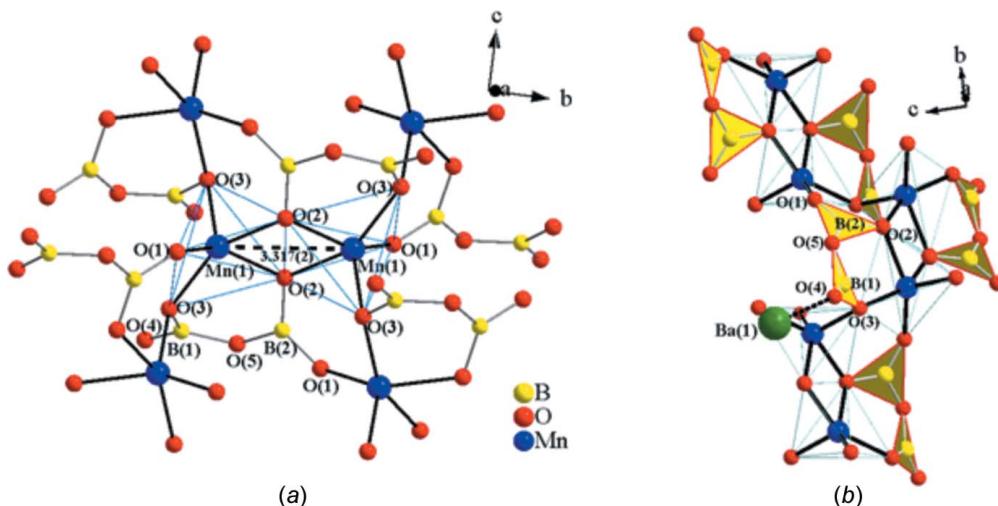
Figure 3
(a) The MnO_5 square pyramids (ball and stick drawing) share a common edge, O2—O2, forming an Mn_2O_8 unit. (b) The $B2O_3$ unit (polyhedral drawing), shares two corners with neighboring MnO_5 square pyramids (ball and stick drawing) through O1 and O2. The only unshared oxygen, O4, of the pyroborate group forms a bond with a Ba atom.

(a)

(c)

(b)

(d)
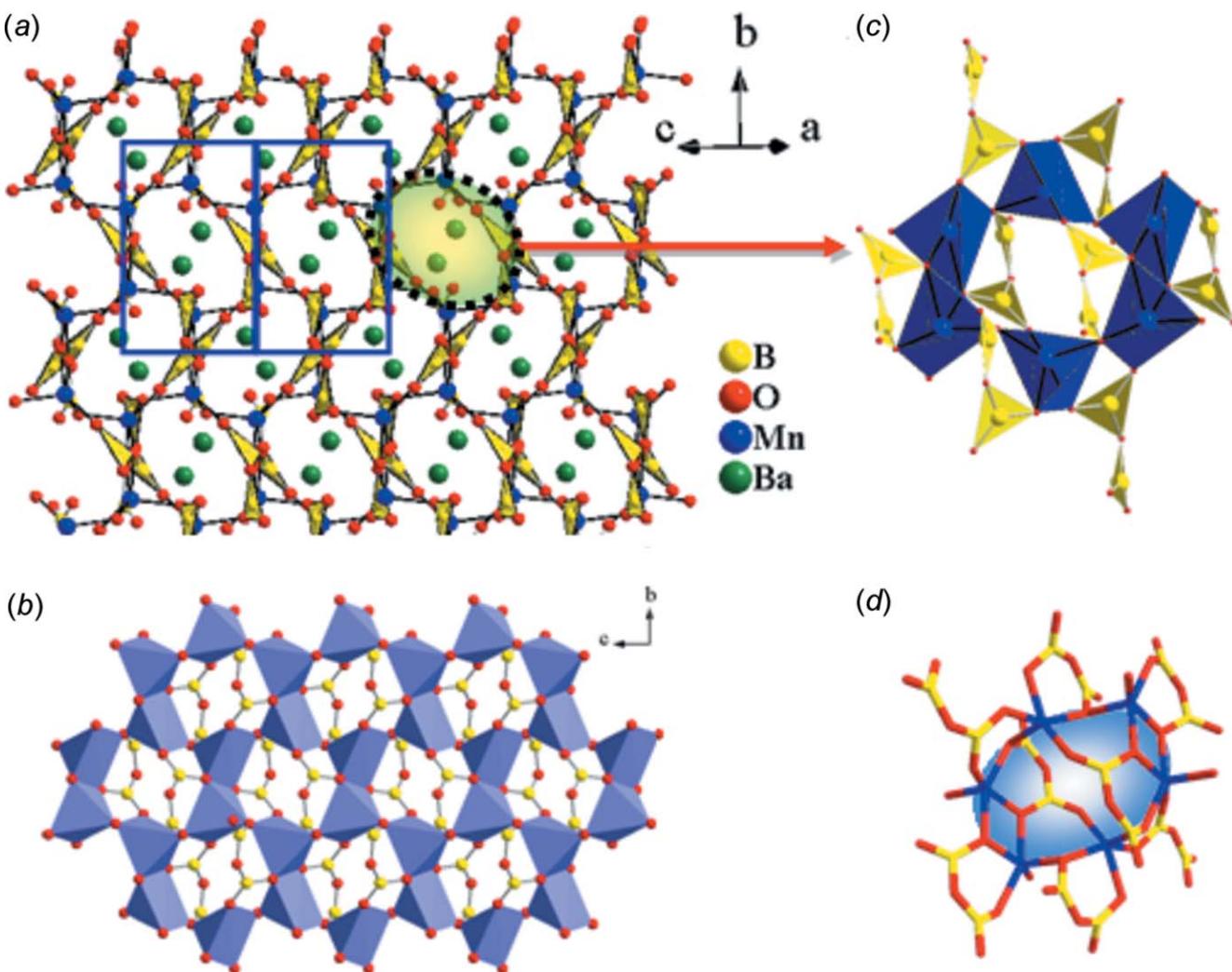
Figure 4
(a) Extended structure of $BaMnB_2O_5$ viewed approximately along the [101] direction. The connectivity of the barium atoms is not shown for clarity. (b) Partial structure of $[MnB_2O_5]^{2-}$ slab viewed along [100] where the polyhedral drawing represents MnO_5 square pyramids and B_2O_5 units are represented by ball-and-stick drawing. (c) Edge-sharing and corner-sharing MnO_5 units corner-share with B_2O_5 pyroborate groups (polyhedral drawing) to create a cage. (d) Stick drawing of one cage with empty space in the middle.
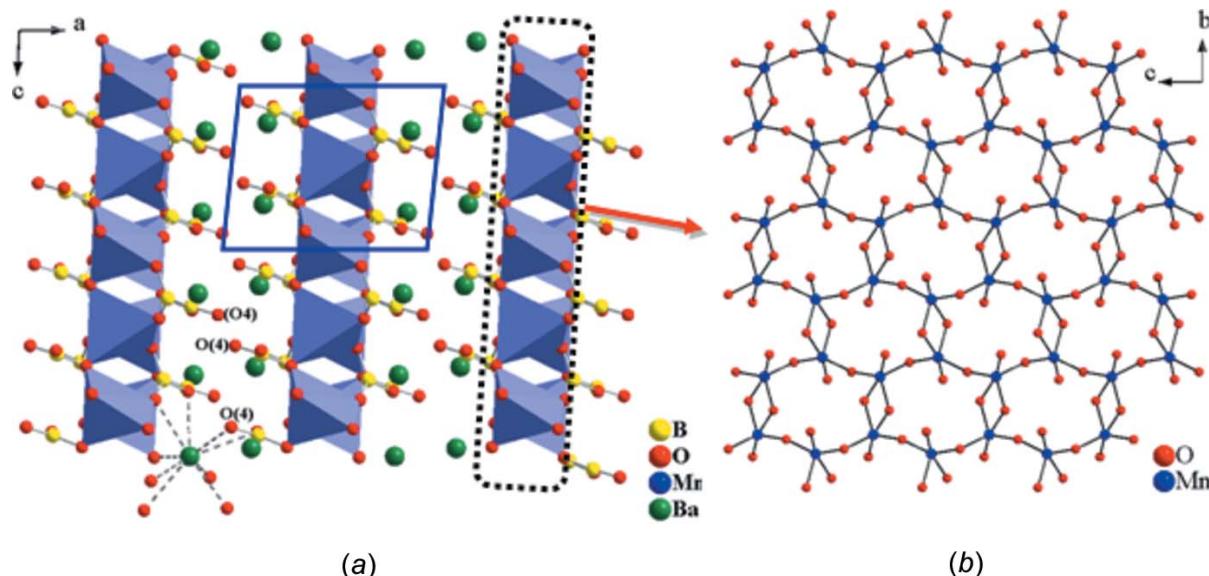
Figure 5
(a) Layered BaMnB$_2$O$_5$ shown by polyhedral and ball-and-stick drawing viewed along the [010] direction. (b) Ball-and-stick drawing of a portion of the manganese oxide network formed by interconnected Mn$_2$O$_8$ dimers by corner sharing.

asymmetry of the bond lengths in the B$_2$O$_5$ group is indicated by slightly varied bond lengths of terminal and bridging B—O bonds. The bridging B—O bond lengths are slightly longer [B1—O5: 1.423 (7); B2—O5: 1.432 (7) Å] than the terminal B—O bond lengths [range 1.332 (8)–1.384 (7) Å]. Notwithstanding, the average B—O bond length (1.380 Å) in the title compound is very close to the corresponding average B—O bond length in BO$_3$ groups in previously reported borates (1.370 Å; Zobetz, 1982). Fig. 1c shows the arrangement of isolated pyroborate units, appearing as two parallel pseudo-one-dimensional chains spiraling around the 2$_1$ axis.

There is one crystallographically independent Mn atom which is coordinated by five oxygen atoms to form a square pyramid with four longer equatorial Mn—O bonds and one short apical Mn—O bond. Fig. 2a shows two Mn1O$_5$ square pyramids sharing a common edge, O2—O2(−x + 1, −y, −z), to form an Mn$_2$O$_8$ unit. As shown in Fig. 3a, Mn atoms are connected to each other via oxygen atoms with a Mn1···Mn1 separation of 3.317 (2) Å and an Mn1—O2—Mn1 angle of 101.23 (16)°. The neighboring Mn$_2$O$_8$ dimers share vertices through oxygen atom O3. The oxygen atom O1 in the Mn$_2$O$_8$ dimer is only corner-shared by the pyroborate group. The only unshared oxygen, O4, of the pyroborate group is pointing into the free space towards the neighboring slabs to form a bond with the barium atom. As shown in Fig. 3b, with respect to the pyroborate group, the B2O$_3$ unit shares two corners with neighboring MnO$_5$ square pyramids through O1 and O2 while the B1O$_3$ unit corner-shares a common oxygen atom, O3, with two other MnO$_5$ square pyramids. This arrangement facilitates the observed curvature which is necessary for the spiral framework found in the extended lattice (Fig. 1b). The unique arrangement of B$_2$O$_5$ groups around the 2$_1$ screw axis provides an essential element allowing the spiral chain to propagate along the b axis. It is well known that the interplanar angle of the B$_2$O$_5$ group is primarily dictated by packing effects and the

nature of the associated cations in the given structure (Thompson et al., 1991). In addition to that, as previously noted, the greater deviations from coplanarity are observed in the arrangement of the B$_2$O$_5$ groups due to variation of the sizes of alkali metals in alkali metal Nb and Ta oxide pyroborates (Akella & Keszler, 1995). Accordingly, the interplanar angle of the B$_2$O$_5$ group is likely to be determined by the associate coordination environment of the barium cations in the title compound. It should be noted that the connectivity of the Mn$_2$O$_8$ and B$_2$O$_5$ structure units would result in a 'dangling' framework unless it can be tightly held together by external bonds. The Ba^{2+} cations, in this case, reside in the spiral framework arranging in zigzag fashion to support and maintain the distance between neighboring [MnB$_2$O$_5$]$^{2-}$ slabs. Coincidentally, this wavy arrangement is critical for the spiral chain to propagate along the b axis. The flexible [MnB$_2$O$_5$]$^{2-}$ framework revolves around Ba^{2+} cations, suggesting a template-like behavior.

The MnO$_5$ units adopt bond lengths normally observed in the Mn^{II} borates. The Mn^{2+}—O bond lengths range from 2.082 (4) to 2.151 (4) Å, comparable with 2.10 Å, the sum of the Shannon crystal radii (Shannon, 1976) for a five coordinated Mn^{2+} (0.89 Å) and two-coordinated O^{2-} (1.21 Å). The bond-valence-sum (BVS) calculations (Brese & O'Keeffe, 1991) for BaMnB$_2$O$_5$ give a valence unit (v.u.) of 2.03 for the Mn^{2+} cation. Based on parameters for B^{3+}—O, bond-valence sums of 2.95 for B1^{3+} and 2.95 for B2^{3+} were calculated. The Ba—O bond lengths are quite diverse, ranging from 2.707 (4) to 2.958 (4) Å. The average Ba—O bond length, 2.83 Å, however matches closely with 2.82 Å, the sum of the Shannon crystal radii for a nine coordinated Ba^{2+} (1.61 Å) and two-coordinated O^{2-} (1.21 Å). The BVS calculation for Ba^{2+} results in 2.08 v.u.

One of the interesting features of the title compound is that the structure can be alternatively viewed as a 'porous'

framework as shown in Fig. 4a. The B_2O_5 units together with interconnected Mn_2O_8 dimers extend along the b axis in a standing wave fashion, creating oval shape windows which also arrange in a zigzag fashion along the same direction. It is intriguing to notice that the two B_2O_5 groups along with the two Mn_2O_8 dimers and two MnO_5 square pyramids create an empty cage (Fig. 4c,d). The polyhedral and ball-and-stick drawing (Fig. 4b) clearly shows the three-dimensional framework bearing large cavities. This unusual structural arrangement is conceivably attributed to the limitation of the size of the pyroborate unit that simultaneously tends to interconnect with barium cations and neighboring Mn_2O_8 dimers in a corner-shared fashion (Fig. 3b). As shown in Fig. 5a, the layered nature of the title compound is characterized by parallel $[MnB_2O_5]^{2-}$ slabs outlined by a dotted rectangle viewed along [010]. Fig. 5b shows the ball-and-stick drawing of a portion of the layered manganese oxide network. Each Mn_2O_8 dimer shares vertices with four other MnO_5 square pyramids through oxygen atoms to form these sheets. Within the extended Mn—O sheet, the MnO_5 square pyramids which share edges are separated from each other by 3.317 (2) Å ($Mn1\cdots Mn1$ distance) whereas those which share corners are separated by 3.435 (1) Å. The distance between the Mn atoms of the adjacent sheets is 8.287 (2) Å. Given the description of the local configuration of the manganese oxide polyhedra, their connectivity along the sheet, and the structural isolation of neighboring Mn—O sheets from each other, one would suspect that the title compound offers opportunities for the study of spin exchange in a confined Mn—O lattice. In theory, a periodic array of well-defined transition metal oxide lattices could provide a useful model for experimental and theoretical developments of magnetic and electronic interactions in transition metal oxides because of their simplified structures (Snyder *et al.*, 2001).

The structure of $BaMnB_2O_5$ is somewhat related to that of triclinic $M_2B_2O_5$ (M = Mn, Sarrat *et al.*, 2005; Fe, Neumair & Huppertz, 2009; Co, Rowsell *et al.*, 2003) phases. The structures of $M_2B_2O_5$ (M = Mn, Fe, Co) phases are based on structurally isolated $[M_4O_{18}]$ tetramers, composed of four octahedra linked by three shared edges, connected through sharing four O—O edges, into ribbons extending along (001) while the boron atoms hold the ribbons together forming B_2O_5 groups. These extended ribbons are parallel to each other and therefore these $M_2B_2O_5$ phases have a quasi-one-dimensional structure in contrast to the two-dimensional Mn—O lattice in the title compound. Magnetic properties have been widely studied for $Co_2B_2O_5$ (Kawano *et al.*, 2010), $Fe_2B_2O_5$ (Kawano *et al.*, 2009), and $Mn_2B_2O_5$ (Fernandes *et al.*, 2003) to understand the low-dimensional interactions derived from the ribbon-like substructures in these compounds. The spin configuration based on the electron-density distribution has been proposed (Sarrat *et al.*, 2005) for $Mn_2B_2O_5$ in which the distance between manganese atoms of adjacent ribbons are 4.526–6.272 Å and electron-density distributions were indicated in the regions between the ribbons. According to their model, all coplanar ribbons of $Mn_2B_2O_5$ are ferromagnetic; their antiferromagnetic behavior is derived from antiparallel

Table 1
Experimental details.

Crystal data	
Chemical formula	$BaMnB_2O_5$
M_r	293.90
Crystal system, space group	Monoclinic, $P2_1/c$
Temperature (K)	300
a, b, c (Å)	8.2868 (17), 8.6570 (17), 6.5263 (13)
β (°)	92.87 (3)
V (Å^3)	467.60 (16)
Z	4
Radiation type	Mo $K\alpha$
μ (mm^{-1})	10.99
Crystal size (mm)	$0.17 \times 0.05 \times 0.02$
Data collection	
Diffractometer	Rigaku AFC8S
Absorption correction	Multi-scan (*REQAB*; Rigaku, 1998)
T_{min}, T_{max}	0.518, 0.808
No. of measured, independent and observed [$I > 2\sigma(I)$] reflections	3807, 830, 777
R_{int}	0.052
$(\sin\theta/\lambda)_{max}$ (Å^{-1})	0.598
Refinement	
$R[F^2 > 2\sigma(F^2)]$, $wR(F^2)$, S	0.025, 0.056, 1.10
No. of reflections	830
No. of parameters	83
$\Delta\rho_{max}$, $\Delta\rho_{min}$ (e Å^{-3})	0.82, −0.98

Computer programs: *CrystalClear* (Rigaku, 2006), *SHELXT* (Sheldrick, 2015a), *SHELXL2014* (Sheldrick, 2015b), *DIAMOND* (Brandenburg, 1999) and *publCIF* (Westrip, 2010).

magnetic orientations between adjacent ribbons. In the title compound, the distance between manganese atoms within the sheets and adjacent sheets are 3.317 (2)–3.435 (1) Å and 8.287 (2) Å, respectively. It is important to note that the Ba^{2+} cations reside in the gap between the two Mn—O sheets. This, together with the greater separation between manganese atoms of adjacent sheets, leads us to believe that magnetic interactions that occur between Mn—O sheets can be extremely weak and the dominant magnetic exchange should be between Mn^{2+} ions within the Mn—O sheet. Judging from the interesting magnetic properties reported for $M_2B_2O_5$ (M = Mn, Fe, Co) compounds, we expect interesting magnetic phenomena from a systematic investigation of the magnetic susceptibility of $BaMnB_2O_5$.

3. Synthesis and crystallization

Light pink crystals of $BaMnB_2O_5$ were grown by employing a CsCl/RbCl flux in a fused silica ampoule under vacuum. MnO (2.74 mmol, 99.999+%, Alfa), BaO (1.37 mmol, 99.99+%, Aldrich) and B_2O_3 (1.37 mmol, 99.98+%, Aldrich) were mixed and ground with the flux (1:3 by weight) in a nitrogen-blanketed drybox. The resulting mixture was heated to 818 K at 1 K min^{-1}, isothermed for two days, heated to 1023 K at 1 K min^{-1}, isothermed for four days, then slowly cooled to 673 K at 0.1 K min^{-1} followed by furnace-cooling to room temperature. Prismatic crystals of $BaMnB_2O_5$ were retrieved upon washing off the solidified melt with deionized water.

4. Refinement

Crystal data, data collection and structure refinement details are summarized in Table 1. The final Fourier difference synthesis showed the maximum residual electron density in the difference Fourier map, 0.82 e $Å^{-3}$, located at 1.19 Å from Ba1 and the minimum, -0.98 e^- $Å^{-3}$, at 0.92 Å from Ba1.

References

Akella, A. & Keszler, D. A. (1995). *J. Solid State Chem.* **120**, 74–79.
Berger, S. V. (1950). *Acta Chem. Scand.* **4**, 1054–1065.
Brandenburg, K. (1999). *DIAMOND*. Crystal Impact GbR, Bonn, Germany.
Brese, N. E. & O'Keeffe, M. (1991). *Acta Cryst.* B**47**, 192–197.
Busche, S. & Bluhm, K. (1995). *Z. Naturforsch. Teil B*, **50**, 1445–1449.
Callegari, A., Mazzi, F. & Tadini, C. (2003). *Eur. J. Miner.* **15**, 277–282.
Fernandes, J. C., Sarrat, F. S., Guimarães, R. B., Freitas, R. S., Continentino, M. A., Doriguetto, A. C., Mascarenhas, Y. P., Ellena, J., Castellano, E. E., Tholence, J. L., Dumas, J. & Ghivelder, L. (2003). *Phys. Rev. B*, **67**, 104413-1-104413-7.
Guo, G.-C., Cheng, W.-D., Chen, J.-T., Huang, J.-S. & Zhang, Q.-E. (1995a). *Acta Cryst.* C**51**, 351–353.
Guo, G.-C., Cheng, W.-D., Chen, J.-T., Zhuang, H.-H., Huang, J.-S. & Zhang, Q.-E. (1995b). *Acta Cryst.* C**51**, 2469–2471.
Heller, G. (1986). *Top. Curr. Chem.* **131**, 39-98.
Hubner, K. H. (1969). *Neues Jahrb. Mineral. Monatsh.* pp. 335–343.
Kawano, T., Morito, H., Yamada, T., Onuma, T., Chichibu, S. F. & Yamane, H. (2009). *J. Solid State Chem.* **182**, 2004–2009.
Kawano, T., Morito, H. & Yamane, H. (2010). *Solid State Sci.* **12**, 1419–1421.
Lin, Q.-S., Cheng, W.-D., Chen, J.-T. & Huang, J.-S. (1999a). *Acta Cryst.* C**55**, 4–6.
Lin, Q.-S., Cheng, W.-D., Chen, J.-T. & Huang, J.-S. (1999b). *J. Solid State Chem.* **144**, 30–34.
Neumair, S. C. & Huppertz, H. (2009). *Z. Naturforsch. Teil B*, **64**, 491–498.
Rigaku (1998). *REQAB*. Rigaku Corporation, Tokyo, Japan.
Rigaku (2006). *CrystalClear*. Rigaku Corporation, Tokyo, Japan.
Rowsell, J. L. C., Taylor, N. J. & Nazar, L. F. (2003). *J. Solid State Chem.* **174**, 189–197.
Sarrat, F. S., Guimarães, R. B., Continentino, M. A., Fernandes, J. C., Doriguetto, A. C. & Ellena, J. (2005). *Phys. Rev. B*, **71**, 224413-1-224413-6.
Shannon, R. D. (1976). *Acta Cryst.* A**32**, 751–767.
Sheldrick, G. M. (2015a). *Acta Cryst.* A**71**, 3–8.
Sheldrick, G. M. (2015b). *Acta Cryst.* C**71**, 3–8.
Simonov, M. A., Egorov-Tismenko, Yu. K., Yamnova, N. A., Belokoneva, E. L. & Belov, N. V. (1980). *Dokl. Akad. Nauk SSSR*, **251**, 1125–1128.
Smith, R. W. & Keszler, D. A. (1997). *J. Solid State Chem.* **129**, 184–188.
Snyder, J., Slusky, J. S., Cava, R. J. & Schiffer, P. (2001). *Nature*, **413**, 48–51.
Thompson, P. D., Huang, J., Smith, R. W. & Keszler, D. A. (1991). *J. Solid State Chem.* **95**, 126–135.
Utzolino, A. & Bluhm, K. (1996). *Z. Naturforsch. Teil B*, **51**, 912–916.
Weil, M. (2003). *Acta Cryst.* E**59**, i95–i97.
Westrip, S. P. (2010). *J. Appl. Cryst.* **43**, 920–925.
Yakubovich, O. V., Yamnova, N. A., Shchedrin, B. M., Simonov, M. A. & Belov, N. V. (1976). *Dokl. Akad. Nauk SSSR*, **228**, 842–845.
Zobetz, E. (1982). *Z. Kristallogr.* **160**, 81–92.

Crystal structure of BaMnB$_2$O$_5$ containing structurally isolated manganese oxide sheets

Elizabeth M. Maschmeyer, Liurukara D. Sanjeewa and Kulugammana G. S. Ranmohotti

Computing details

Data collection: *CrystalClear* (Rigaku, 2006); cell refinement: *CrystalClear* (Rigaku, 2006); data reduction: *CrystalClear* (Rigaku, 2006); program(s) used to solve structure: SHELXT (Sheldrick, 2015a); program(s) used to refine structure: *SHELXL2014* (Sheldrick, 2015b); molecular graphics: *DIAMOND* (Brandenburg, 1999); software used to prepare material for publication: *publCIF* (Westrip, 2010).

Barium manganese(II) pyroborate

Crystal data

BaMnB$_2$O$_5$	$F(000) = 524$
$M_r = 293.90$	$D_x = 4.175$ Mg m^{-3}
Monoclinic, $P2_1/c$	Mo $K\alpha$ radiation, $\lambda = 0.71073$ Å
$a = 8.2868$ (17) Å	Cell parameters from 3139 reflections
$b = 8.6570$ (17) Å	$\theta = 3.1–29.6°$
$c = 6.5263$ (13) Å	$\mu = 10.99$ mm^{-1}
$\beta = 92.87$ (3)°	$T = 300$ K
$V = 467.60$ (16) Å^3	Prismatic, pink
$Z = 4$	$0.17 \times 0.05 \times 0.02$ mm

Data collection

Rigaku AFC8S diffractometer	830 independent reflections
Radiation source: fine-focus sealed tube	777 reflections with $I > 2\sigma(I)$
ω scans	$R_{int} = 0.052$
Absorption correction: multi-scan (*REQAB*; Rigaku, 1998)	$\theta_{max} = 25.2°$, $\theta_{min} = 3.4°$
	$h = -9 \rightarrow 9$
	$k = -10 \rightarrow 10$
$T_{min} = 0.518$, $T_{max} = 0.808$	$l = -7 \rightarrow 7$
3807 measured reflections	1 standard reflections every 1 reflections

Refinement

Refinement on F^2	$w = 1/[\sigma^2(F_o^2) + (0.0315P)^2]$
Least-squares matrix: full	where $P = (F_o^2 + 2F_c^2)/3$
$R[F^2 > 2\sigma(F^2)] = 0.025$	$(\Delta/\sigma)_{max} = 0.005$
$wR(F^2) = 0.056$	$\Delta\rho_{max} = 0.82$ e Å^{-3}
$S = 1.10$	$\Delta\rho_{min} = -0.98$ e Å^{-3}
830 reflections	Extinction correction: SHELXL2014 (Sheldrick, 2015b),
83 parameters	Fc*=kFc[1+0.001xFc$^2\lambda^3$/sin(2θ)]$^{-1/4}$
0 restraints	Extinction coefficient: 0.0061 (7)

Special details

Geometry. All esds (except the esd in the dihedral angle between two l.s. planes) are estimated using the full covariance matrix. The cell esds are taken into account individually in the estimation of esds in distances, angles and torsion angles; correlations between esds in cell parameters are only used when they are defined by crystal symmetry. An approximate (isotropic) treatment of cell esds is used for estimating esds involving l.s. planes.

Fractional atomic coordinates and isotropic or equivalent isotropic displacement parameters ($Å^2$)

	x	y	z	U_{iso}*/U_{eq}
Ba1	0.14891 (4)	0.07969 (4)	0.22488 (5)	0.00932 (16)
Mn1	0.53148 (10)	0.18805 (10)	0.02929 (12)	0.0087 (2)
B1	0.1784 (8)	−0.2828 (7)	0.1447 (10)	0.0100 (13)
B2	0.2960 (8)	0.4492 (7)	0.1980 (10)	0.0115 (13)
O1	0.3314 (5)	0.3308 (4)	0.0723 (6)	0.0133 (9)
O2	0.3587 (5)	0.0300 (4)	−0.1080 (6)	0.0126 (9)
O3	0.3228 (5)	−0.2185 (4)	0.2184 (6)	0.0106 (8)
O4	0.0457 (5)	−0.2018 (4)	0.0939 (6)	0.0110 (8)
O5	−0.1725 (5)	0.0536 (4)	0.3763 (6)	0.0109 (8)

Atomic displacement parameters ($Å^2$)

	U^{11}	U^{22}	U^{33}	U^{12}	U^{13}	U^{23}
Ba1	0.0103 (2)	0.0088 (2)	0.0088 (2)	0.00002 (12)	−0.00031 (13)	−0.00026 (13)
Mn1	0.0094 (5)	0.0080 (4)	0.0086 (5)	0.0000 (3)	−0.0006 (3)	−0.0001 (3)
B1	0.006 (3)	0.013 (3)	0.011 (3)	−0.002 (3)	0.000 (2)	0.002 (3)
B2	0.010 (3)	0.011 (3)	0.014 (3)	0.005 (3)	0.000 (3)	−0.003 (3)
O1	0.012 (2)	0.015 (2)	0.013 (2)	0.0056 (17)	−0.0030 (17)	−0.0054 (17)
O2	0.017 (2)	0.0073 (18)	0.012 (2)	−0.0008 (16)	−0.0055 (17)	−0.0004 (16)
O3	0.0108 (19)	0.0109 (19)	0.010 (2)	−0.0023 (16)	−0.0002 (16)	0.0011 (16)
O4	0.012 (2)	0.009 (2)	0.012 (2)	0.0033 (16)	0.0004 (16)	−0.0018 (16)
O5	0.013 (2)	0.0075 (19)	0.012 (2)	0.0010 (16)	−0.0036 (16)	0.0006 (16)

Geometric parameters (Å, º)

Ba1—O4	2.707 (4)	Mn1—O1	2.098 (4)
Ba1—O1[i]	2.772 (4)	Mn1—O2	2.144 (4)
Ba1—O4[ii]	2.777 (4)	Mn1—O2[v]	2.147 (4)
Ba1—O4[iii]	2.787 (4)	Mn1—O3[vi]	2.151 (4)
Ba1—O5[iv]	2.845 (4)	B1—O4	1.332 (8)
Ba1—O1	2.855 (4)	B1—O3	1.384 (7)
Ba1—O2	2.882 (4)	B1—O5[vii]	1.423 (7)
Ba1—O5	2.896 (4)	B2—O1	1.354 (7)
Ba1—O3	2.958 (4)	B2—O2[i]	1.357 (8)
Mn1—O3[v]	2.082 (4)	B2—O5[iii]	1.432 (7)
O4—Ba1—O1[i]	131.36 (11)	O1—Mn1—O2[v]	144.52 (16)
O4—Ba1—O4[ii]	86.77 (11)	O2—Mn1—O2[v]	78.77 (16)
O1[i]—Ba1—O4[ii]	141.16 (11)	O3[v]—Mn1—O3[vi]	102.81 (15)

O4—Ba1—O4^{iii}	124.37 (5)	O1—Mn1—O3^{vi}	95.36 (15)
O1^{i}—Ba1—O4^{iii}	76.50 (12)	O2—Mn1—O3^{vi}	153.85 (15)
O4^{ii}—Ba1—O4^{iii}	74.51 (8)	O2^{v}—Mn1—O3^{vi}	86.12 (14)
O4—Ba1—O5^{iv}	85.98 (11)	O1—B2—O2^{i}	125.6 (5)
O1^{i}—Ba1—O5^{iv}	49.87 (11)	O1—B2—O5^{iii}	116.5 (5)
O4^{ii}—Ba1—O5^{iv}	148.29 (11)	O2^{i}—B2—O5^{iii}	117.8 (5)
O4^{iii}—Ba1—O5^{iv}	84.37 (11)	B2—O1—Mn1	136.3 (4)
O4—Ba1—O1	137.70 (12)	B2—O1—Ba1^{viii}	99.1 (3)
O1^{i}—Ba1—O1	78.21 (9)	Mn1—O1—Ba1^{viii}	117.24 (16)
O4^{ii}—Ba1—O1	75.33 (12)	B2—O1—Ba1	103.3 (3)
O4^{iii}—Ba1—O1	87.65 (11)	Mn1—O1—Ba1	91.97 (13)
O5^{iv}—Ba1—O1	127.91 (11)	Ba1^{viii}—O1—Ba1	102.80 (13)
O4—Ba1—O2	79.67 (11)	B2^{viii}—O2—Mn1	121.5 (4)
O1^{i}—Ba1—O2	109.48 (11)	B2^{viii}—O2—Mn1^{v}	118.6 (4)
O4^{ii}—Ba1—O2	80.88 (11)	Mn1—O2—Mn1^{v}	101.23 (16)
O4^{iii}—Ba1—O2	143.59 (11)	B2^{viii}—O2—Ba1	117.8 (4)
O5^{iv}—Ba1—O2	127.79 (11)	Mn1—O2—Ba1	90.29 (13)
O1—Ba1—O2	60.05 (11)	Mn1^{v}—O2—Ba1	102.44 (14)
O4—Ba1—O5	75.88 (11)	B1—O3—Mn1^{v}	107.8 (4)
O1^{i}—Ba1—O5	102.48 (11)	B1—O3—Mn1^{ix}	123.9 (3)
O4^{ii}—Ba1—O5	77.04 (12)	Mn1^{v}—O3—Mn1^{ix}	108.48 (17)
O4^{iii}—Ba1—O5	49.20 (11)	B1—O3—Ba1	86.7 (3)
O5^{iv}—Ba1—O5	71.25 (13)	Mn1^{v}—O3—Ba1	101.68 (14)
O1—Ba1—O5	133.67 (10)	Mn1^{ix}—O3—Ba1	124.92 (15)
O2—Ba1—O5	147.72 (11)	B1—O4—Ba1	98.7 (3)
O4—Ba1—O3	49.93 (11)	B1—O4—Ba1^{ii}	145.9 (4)
O1^{i}—Ba1—O3	90.55 (11)	Ba1—O4—Ba1^{ii}	93.23 (11)
O4^{ii}—Ba1—O3	125.91 (11)	B1—O4—Ba1^{vii}	91.4 (3)
O4^{iii}—Ba1—O3	153.01 (10)	Ba1—O4—Ba1^{vii}	131.11 (15)
O5^{iv}—Ba1—O3	69.38 (11)	Ba1^{ii}—O4—Ba1^{vii}	104.46 (13)
O1—Ba1—O3	113.11 (11)	B1^{iii}—O5—B2^{vii}	125.1 (5)
O2—Ba1—O3	63.01 (10)	B1^{iii}—O5—Ba1^{iv}	119.5 (3)
O5—Ba1—O3	113.20 (11)	B2^{vii}—O5—Ba1^{iv}	93.9 (3)
O3^{v}—Mn1—O1	121.48 (15)	B1^{iii}—O5—Ba1	85.3 (3)
O3^{v}—Mn1—O2	99.07 (15)	B2^{vii}—O5—Ba1	126.0 (3)
O1—Mn1—O2	85.17 (16)	Ba1^{iv}—O5—Ba1	108.75 (13)
O3^{v}—Mn1—O2^{v}	92.39 (15)		

Symmetry codes: (i) *x*, −*y*+1/2, *z*+1/2; (ii) −*x*, −*y*, −*z*; (iii) −*x*, *y*+1/2, −*z*+1/2; (iv) −*x*, −*y*, −*z*+1; (v) −*x*+1, −*y*, −*z*; (vi) −*x*+1, *y*+1/2, −*z*+1/2; (vii) −*x*, *y*−1/2, −*z*+1/2; (viii) *x*, −*y*+1/2, *z*−1/2; (ix) −*x*+1, *y*−1/2, −*z*+1/2.